Magn Reson Mater Phy (2015) 28:119–126
DOI 10.1007/s10334-014-0447-2

RESEARCH ARTICLE

Effect of acute hyperglycemia on moderately hypothermic GL261 mouse glioma monitored by T1-weighted DCE MRI

Rui V. Simões · Juan E. Ortuño · Louisa Bokacheva · Ana P. Candiota · Maria J. Ledesma-Carbayo · Teresa Delgado-Goñi · Maria L. García-Martín · Andrés Santos · Carles Arús

Received: 29 November 2013 / Revised: 15 April 2014 / Accepted: 15 April 2014 / Published online: 11 June 2014

Abstract
Objective We sought to evaluate the effects of acute hyperglycemia induced by intraperitoneal injection of glucose (2.7 g/kg) on vascular delivery to GL261 mouse gliomas kept at moderate hypothermia ($\sim$30 °C).
Materials and methods Seven GL261 glioma-bearing mice were studied by T1-weighted DCE MRI before and after an injection of glucose ($n = 4$) or saline ($n = 3$). Maximum relative contrast enhancement (RCE) and initial area under the enhancement curve (IAUC) were determined in each pixel.
Results The mean tumor parameter values showed no significant changes after injecting either saline (RCE -5.9 ± 5.0 %; IAUC -3.7 ± 3.6 %) or glucose (RCE -1.6 ± 9.0 %; IAUC $+0.6 \pm 6.4$ %). Pixel-by-pixel analysis revealed small post-injection changes in RCE and IAUC between the glucose and saline groups, all within 13 % range of their baseline values.
Conclusion Perturbing the metabolism of GL261 tumors kept at moderate hypothermia with hyperglycemia did not induce significant changes in the permeability/perfusion of these tumors. This is relevant for future studies with this model since regional differences in glucose accumulation could thus reflect basal heterogeneities in vasculature and/or metabolism of GL261 tumors.

Keywords Acute hyperglycemia · Brain tumor · Contrast agent · GL261 cells · Model-free quantification · Moderate hypothermia · Perfusion · Permeability

R. V. Simões · A. P. Candiota · T. Delgado-Goñi · C. Arús (✉)
Departament de Bioquímica i Biologia Molecular, Facultat de Biociències, Universitat Autònoma de Barcelona, 08193 Cerdanyola del Vallès, Spain
e-mail: Carles.Arus@uab.cat

R. V. Simões
e-mail: portasferre@clinic.ub.es

R. V. Simões · J. E. Ortuño · A. P. Candiota · M. J. Ledesma-Carbayo · T. Delgado-Goñi · A. Santos · C. Arús
Centro de Investigación Biomédica en Red – Bioingeniería, Biomateriales y Nanomedicina (CIBER-BBN), Zaragoza, Spain

Present Address:
R. V. Simões
Department of Maternal-Fetal Medicine (ICGON), Clinic Hospital, University of Barcelona, 08028 Barcelona, Spain

J. E. Ortuño · M. J. Ledesma-Carbayo · A. Santos
Tecnología de Imágenes Biomédicas, Universidad Politécnica de Madrid, 28040 Madrid, Spain

L. Bokacheva
Department of Medical Physics, Memorial Sloan-Kettering Cancer Center, New York, NY, USA

A. P. Candiota · C. Arús
Institut de Biotecnologia i de Biomedicina, Universitat Autònoma de Barcelona, 08193 Cerdanyola del Vallès, Spain

Present Address:
T. Delgado-Goñi
Division of Radiotherapy and Imaging, Cancer Research UK and EPSRC Cancer Imaging Centre, The Royal Marsden NHS Foundation Trust, The Institute of Cancer Research, Sutton, Surrey SM2 5PT, UK

M. L. García-Martín
Nanobiotechnology Area, Andalusian Center for Nanomedicine and Biotechnology (BIONAND), Málaga, Spain

Abbreviations

DCE Dynamic contrast enhancement
IAUC Initial area under the curve
MRSI Magnetic resonance spectroscopic imaging
RCE Relative contrast enhancement
TBF Tumor blood flow

Introduction

Mouse models of high grade glioma are important tools to study aggressive human brain tumors and have been extensively evaluated by magnetic resonance imaging (MRI) [1]. Glucose metabolism is markedly enhanced in gliomas compared to normal brain parenchyma, and recent in vivo magnetic resonance spectroscopic imaging (MRSI) studies show its heterogeneity in different regions of the tumor. Thus, C6 rat gliomas have regional differences in the distributions of lactate and extracellular acidity, both before and during the glucose infusion [2]. Glycolysis has also been found to be consistently more prominent in hypoxic areas of human gliomas in mice than in regions of diffuse infiltrative growth [3]. Taking into account these differences, a new method has been proposed to improve tumor grading in vivo—perturbing the basal MRSI metabolic pattern of mouse gliomas with acute hyperglycemia [4]. This method showed (1) higher glucose uptake and (2) regional differences in glucose accumulation in GL261 gliomas than in normal brain parenchyma, after intraperitoneal injection of glucose in mice under moderate brain hypothermia ($\sim$30 °C) [5, 6].

Intraperitoneal administration of hyperosmolar solutions, such as glucose and mannitol, significantly decreases tumor blood flow (TBF) [7]. In subcutaneous rat tumors, TBF was shown to decrease by 80 % in radiation-induced fibrosarcoma 1 (RIF-1) [8], by up to 100 % in Yoshida sarcoma [9], and by about 60 % in Walker 256 carcinoma [10]. As shown in Yoshida sarcomas, the decrease in the TBF leads to the reduction in glycolysis and respiration, which may explain the temperature decrease seen in Walker 256 carcinomas, from 37 to 30.5 °C [11]. Altogether, these studies indicate that systemic delivery to subcutaneous tumors became impaired during intraperitoneally induced hyperglycemia.

It remains unclear whether the regional differences in glucose accumulation seen in GL261 tumors [6] are due to basal heterogeneities in vasculature and/or metabolism of each tumor [12], or to the effects of acute hyperglycemia on local blood supply to the tumor. To ascertain this, in this study we used T1-weighted dynamic contrast-enhanced (DCE) MRI to investigate the effect of acute hyperglycemia on vascular supply and permeability of GL261 mouse gliomas, during moderate brain hypothermia.

Materials and methods

Mice and brain tumors

Seven C57BL/6 female mice, weighing 20–22 g, were used in this study. Mice were obtained from Charles River Laboratories (L'Arbresle Cedex, France) and housed at the animal facility of the Universitat Autònoma de Barcelona, Spain. All animal studies were approved by the local ethics committee in accordance with the regional and state legislation (DARP-4600/CEEAH-530). GL261 mouse glioma cells were obtained from the Tumor Bank Repository at the National Cancer Institute (Frederick, MD, USA) and grown in vitro. Tumors were initiated by intracranial stereotactic injection of 10^5 tumor cells in the caudate nucleus of each mouse, as previously described [6]. Tumors were allowed to grow for 2–3 weeks, until they reached 25–60 mm^3 volume, and were then imaged with MRI.

Animal preparation

For the imaging studies, mice were anesthetized with isoflurane (1–2 % in air). An i.p. cannula was placed for the injection of glucose or saline (sham injection) [10]. For contrast agent administration, the tail vein was cannulated with a 30G syringe needle attached to Teflon tubing, filled with 35 μL of heparinized saline solution (40 U/mL). This tubing was connected to a home-built two-way polyethylene tubing system filled with heparinized saline, and either contrast agent (gadopentetate dimeglumine, Magnevist, Bayer Schering Pharma AG, Berlin, Germany; 50 mM in saline) or saline solution (0.9 % NaCl). Throughout the imaging experiments, respiration and body temperature were constantly monitored (SA Instruments, Inc., New York, USA), and maintained at a normal rate of 60–80 breaths/min and 28.5–29.5 °C, respectively. The body temperature was controlled with a recirculating water blanket.

MRI

MRI studies were performed at the joint NMR facility of the Universitat Autònoma de Barcelona and CIBER-BBN (Cerdanyola del Vallès, Spain), using a 7 T horizontal system, *BioSpec 70/30* (Bruker BioSpin, Ettlingen, Germany) running Bruker ParaVision 4.0 software and equipped with B-GA20S gradients and a quadrature receive surface coil actively decoupled from a linear mini-imaging resonator with 72 mm inner diameter. Mice were positioned inside the

magnet, and the locations of the brain tumors were first detected using fast T2-weighted images (Rapid Acquisition with Relaxation Enhancement sequence, RARE). The DCE MRI examination was then conducted as previously described [13]. Three pre-contrast images were acquired, after which a bolus of contrast agent was manually injected (0.2 mmol/kg, 4 mL/kg, 10–15 s duration). A series of 41 dynamic images was acquired with the multi-slice multi-echo (MSME) sequence, with the following parameters: TR/TE, 200/9 ms; number of averages, 2; field of view, 17.6 × 17.6 mm^2; slice thickness, 1 mm; in-plane resolution, 138 × 138 μm/pixel; interslice distance, 1.1 mm; number of slices, 3; temporal resolution, 51.2 s per frame; 41 frames; total acquisition time, 35 min. After the completion of the DCE MRI study, animals were kept inside the magnet for about 4 h, until visual examination of the T1-weighted images confirmed that the contrast agent had washed out from the brain. During that period, animals received a small i.v. bolus (30–40 μL) of heparinized saline every 45–60 min, to prevent blood from clotting in the cannula. When contrast enhancement was no longer seen in the brain, four randomly chosen mice were given a 10 mL/kg bolus injection of D-glucose (1.4 M in saline) and three control mice received sham saline solution (10 mL/kg). At 88 min after the injection of either glucose or saline, the DCE examination was repeated with the same parameters as the first DCE acquisition. The time-point for DCE-MRI was chosen based on our previous results with the same experimental model [6], i.e., when blood glucose was ~23 mM (compared to basal levels of ~5 mM) and its levels had increased up to sixfold in the tumor. The total duration of the protocol for each animal was about 7 h. After the second DCE MRI study, mice were sacrificed with an intraperitoneal injection of pentobarbital (200 mg/kg, 60 mg/mL).

Data analysis

T2-weighted images were used to calculate the tumor volume for each mouse, as described before [14]: the tumor regions were individually selected in each slice using manually defined regions of interest (ROI); the given areas for each ROI were then added and multiplied by the inter-slice distance.

DCE MRI data were processed using an in-house developed software [15]. For each animal, regions of interest (ROIs) were manually drawn around the tumor on every slice. All dynamic data sets were downsampled in-plane from 128 × 128 to 64 × 64 pixels, by averaging 2 × 2 pixels into one final pixel, in order to improve the signal-to-noise ratio. Signal enhancement was calculated in each tumor pixel as the ratio of the pixel signal intensity to the mean pre-contrast signal. Relative contrast enhancement (RCE) maps were constructed by finding the maximum enhancement in each pixel. Pixels with noisy enhancement curves were excluded by applying an empirical threshold: the square root of the sum of squares of residuals above 3.5 % of the RCE. Maps of the initial area under the curve (IAUC) were generated by integrating the enhancement curves during the first 154 s after the contrast agent administration [16, 17].

Table 1 Average pixel-by-pixel RCE and IAUC values for each tumor studied (1–7), including mean ± SD values per group, and respective post/pre-injection percent changes. Analyses of the mean parameter values per tumor showed no significant differences between pre- and post-injection cases, for either saline or glucose, according to both the Wilcoxon test and the paired *t* test. The Mann–Whitney *U* test also did not reveal differences in post/pre-injection changes between saline and glucose groups, for each of the three parameters analyzed and for tumor volumes

	Tumors (T#)			
Saline	T1	T2	T3	Average
Volume (mm^3)	54.0	41.2	28.1	41.1 ± 13.0
RCE (%)				
Pre	183.3 ± 12.9	154.0 ± 14.4	209.3 ± 23.4	182.2 ± 27.6
Post	181.4 ± 13.4	145.1 ± 14.0	185.5 ± 20.5	170.7 ± 22.2
Change (%)	−1.0 ± 4.3	−5.7 ± 4.5	−11.0 ± 7.1	**−5.9 ± 5.0**
IAUC (A.U.)				
Pre	3.7 ± 0.2	3.4 ± 0.3	3.9 ± 0.6	3.7 ± 0.3
Post	3.7 ± 0.2	3.2 ± 0.3	3.7 ± 0.5	3.5 ± 0.3
Change (%)	0.4 ± 4.0	−5.3 ± 4.7	−6.1 ± 9.8	**−3.7 ± 3.6**
Glucose	T4	T5	T6	T7	Average
Volume (mm^3)	61.1	56.3	25.8	32.9	44.0 ± 17.3
RCE (%)					
Pre	177.8 ± 13.6	162.8 ± 12.0	167.4 ± 15.9	198.3 ± 17.2	176.5 ± 15.8
Post	193.0 ± 17.3	163.2 ± 10.7	162.4 ± 17.2	172.6 ± 19.0	172.8 ± 14.2
Change (%)	8.7 ± 7.1	0.5 ± 5.5	−2.8 ± 8.0	−13.0 ± 5.2	**−1.6 ± 9.0**
IAUC (A.U.)					
Pre	3.6 ± 0.2	3.6 ± 0.3	3.6 ± 0.3	3.8 ± 0.4	3.7 ± 0.1
Post	3.9 ± 0.3	3.6 ± 0.2	3.5 ± 0.3	3.5 ± 0.4	3.6 ± 0.2
Change (%)	6.6 ± 6.9	3.6 ± 5.8	0.4 ± 8.6	−8.1 ± 5.9	**0.6 ± 6.4**

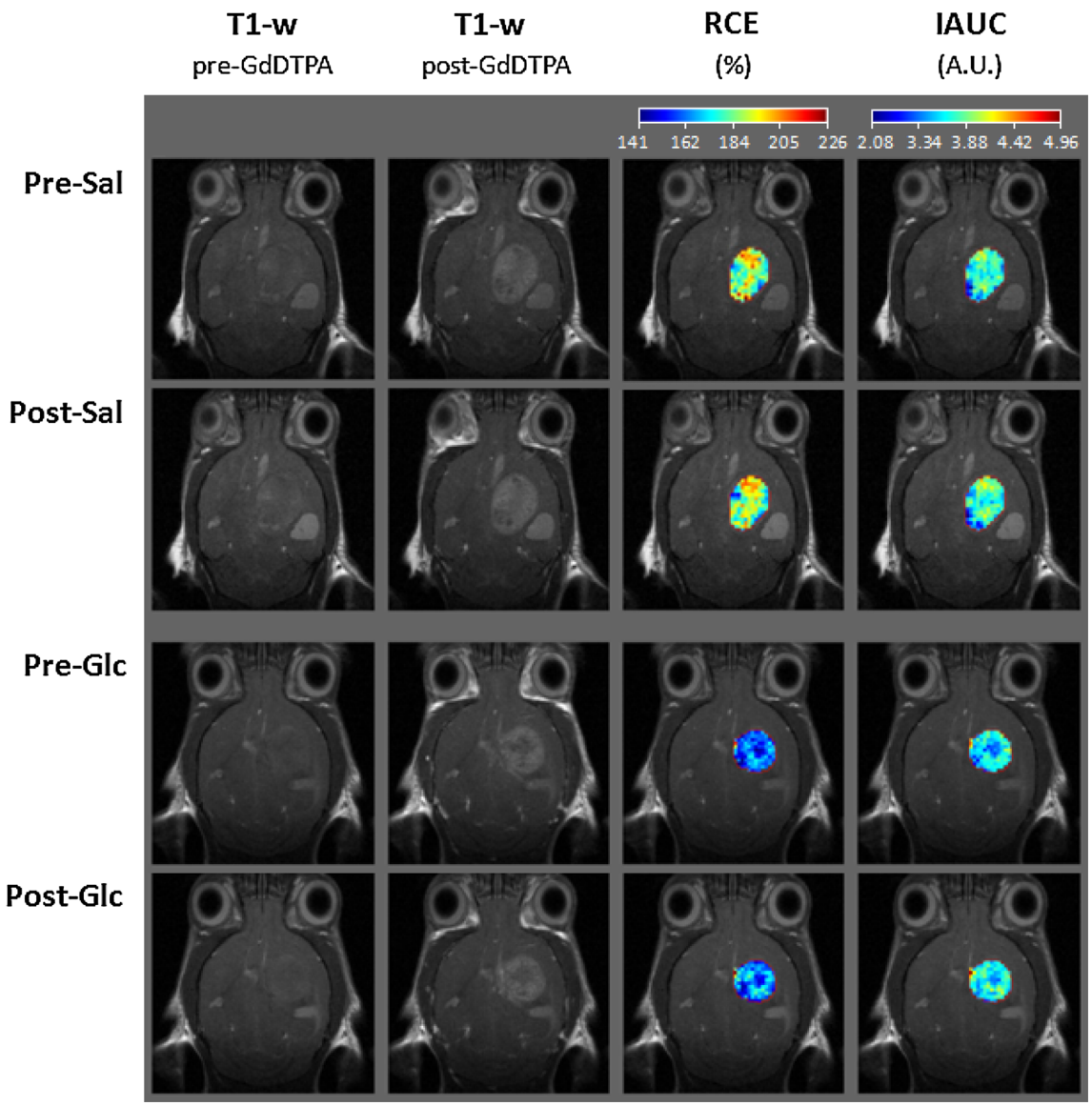

Fig. 1 T1-weighted (T1-w) images and parametric maps for two mice, displayed with original resolution of 128 × 128 pixels. *Top row*: tumor (T2, 41.2 mm^3) studied before and after a sham saline injection (Sal). *Bottom row*: tumor (T5, 56.3 mm^3) studied after an injection of glucose (Glc). A single slice is displayed for each animal. From *left* to *right*: pre-contrast T1-w images, T1-w images at 51.2 s after injection of contrast agent, RCE maps (%) and IAUC maps (arbitrary units, A.U.). The *color bar scales* for each parameter are the same for both mice

Regression plots, histograms and box-plots were generated in Matlab R2009b (MathWorks, Natick MA, USA).

Statistical analysis

Statistical analyses were carried out in SPSS *15.0* (SPSS Inc., Chicago IL, USA). The changes in tumor parameters after the injection of glucose or saline were calculated pixel-by-pixel and expressed as percentages of the pre-injection parameter values. Average tumor MRI parameters before (pre) and MRI parameters after (post) injection were compared within the saline and glucose groups, using both the Wilcoxon test and the paired *t* test. The Mann–Whitney *U* test was used to evaluate the significance of percent parameter changes and tumor sizes between glucose and saline groups. Parameter correlations before and after injection were evaluated with Spearman's correlation coefficient ρ. The significance level for all tests was $p < 0.05$.

Results

A total of seven tumors were studied, three with saline challenge and four with glucose challenge. Tumor volumes ranged from 26 to 61 mm^3, as detailed in Table 1, and no significant differences in volume were detected between

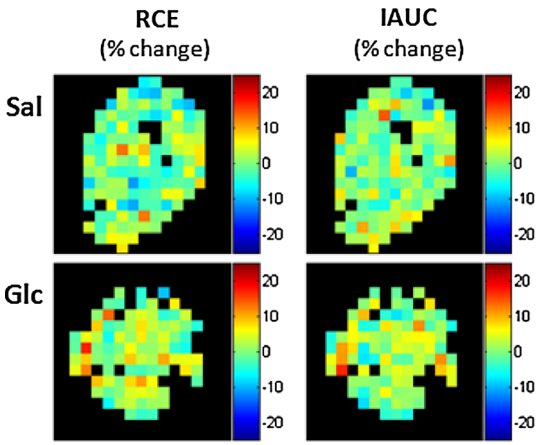

Fig. 2 Maps of relative pixel changes (%) for RCE and IAUC after glucose injection. Resolution downsized compared to the respective parametric maps shown in Fig. 1. Pixels in black were discarded from analysis, as explained in "Methods" section

saline and glucose groups. The enhancement parameters varied in the following ranges in all seven tumors: RCE, 120–250 %; IAUC, 2.7–5.0 A.U. None of the tumors showed signs of bulk necrosis, which in GL261 typically develops around the third and fourth week after implantation [18]. The mean parameter values did not correlate with tumor size. At baseline, smaller tumors appeared to be more heterogeneous (Table 1), as indicated by the correlations between the parameter standard deviations and tumor volumes: RCE, $\rho = -0.79$ ($p = 0.048$); IAUC, $\rho = -0.86$ ($p = 0.024$).

Examples of RCE and IAUC maps are shown in Fig. 1, before and after saline and glucose injections. The spread of pixel intensities in the pre-injection maps illustrates the vascular heterogeneity within each tumor and also between the two tumors shown. However, the magnitude and the spatial distributions of RCE and IAUC remained essentially unchanged after the injection of either saline or glucose. The maps of parameter changes, shown in Fig. 2, indicate that post-injection changes are within $\sim$10 % range for RCE and IAUC.

The correlation plots between pre-injection and post-injection parameter values and the histograms of IAUC are shown in Fig. 3 for all tumors investigated. The mean parameters for each tumor and within groups are summarized in Table 1. The correlation plots show that RCE and IAUC changed concordantly after injection ($\rho \geq 0.5$). The correlation plots indicate that the saline and glucose challenges did not cause well-pronounced changes within each group. In the saline group, one tumor (T1) showed virtually no changes, and two tumors showed a slight decrease in post-injection parameters (T2 and T3). In the glucose group, two tumors showed minimal changes (T5 and T6, less than 5 % changes in RCE and IAUC); one tumor showed a slight increase (T4: RCE, 8.7 %; IAUC, 6.6 %) and another one a decrease in enhancement parameters (T7). Interestingly, the larger decreases in tumor parameters (up to −13 %) were observed in heterogeneous tumors T3 and T7, both with higher RCE and IAUC values in the center and lower ones in the periphery. The remaining tumors, including tumor T4, in which the parameter values increased after glucose challenge, exhibited relatively homogeneous spatial parameter distributions.

The box-plots show small and comparable post-injection changes in RCE and IAUC. The average RCE and IAUC parameter changes detected in saline and glucose groups were within 13 % range of the initial values and there were no significant differences between the two groups according to the Mann–Whitney *U* test (Fig. 4).

Discussion

In this work, we have studied GL261 brain tumors with DCE MRI, before and after intraperitoneal injections of saline and glucose. Similarly to the observations of Cha et al. [18], in our study GL261 gliomas showed avid enhancement on T1-weighted post-contrast images since week one after implantation, even though these tumors do not develop angiogenesis until week three. The T1 contrast enhancement indicates that the blood–brain barrier in these tumors is disrupted even at the earliest stages of tumor growth. As a result, the contrast enhancement of these tumors likely reflects a combination of perfusion and permeability. Specifically, the upslopes of the DCE-MRI curves are typically highly dependent on perfusion [19].

The two parameters used here to characterize tumor vascular delivery and permeability, RCE and IAUC, provided related information. The RCE values characterize the overall amplitude of enhancement without distinguishing the time point when the maximum occurs [20]. Thus, RCE does not distinguish pixels with a washout enhancement type, in which the maximum is reached within the first 2–3 min after injection (well perfused regions), from pixels with persistent enhancement, in which the maximum occurs towards the end of experiment (poorly perfused regions). On the other hand, IAUC characterizes only the early part of the enhancement and contains information mainly about perfusion and vascular volume in addition to contributions from permeability and leakage volume.

The post-injection changes in RCE and IAUC parameters were small in all tumors studied. Tumors with the highest and most heterogeneous baseline perfusion/permeability parameters (T3 in saline group; and T7 in glucose group) showed the largest decrease in RCE and IAUC after injection (up to 13 %). Thus, the injection of saline or glucose appeared to induce only small variations of

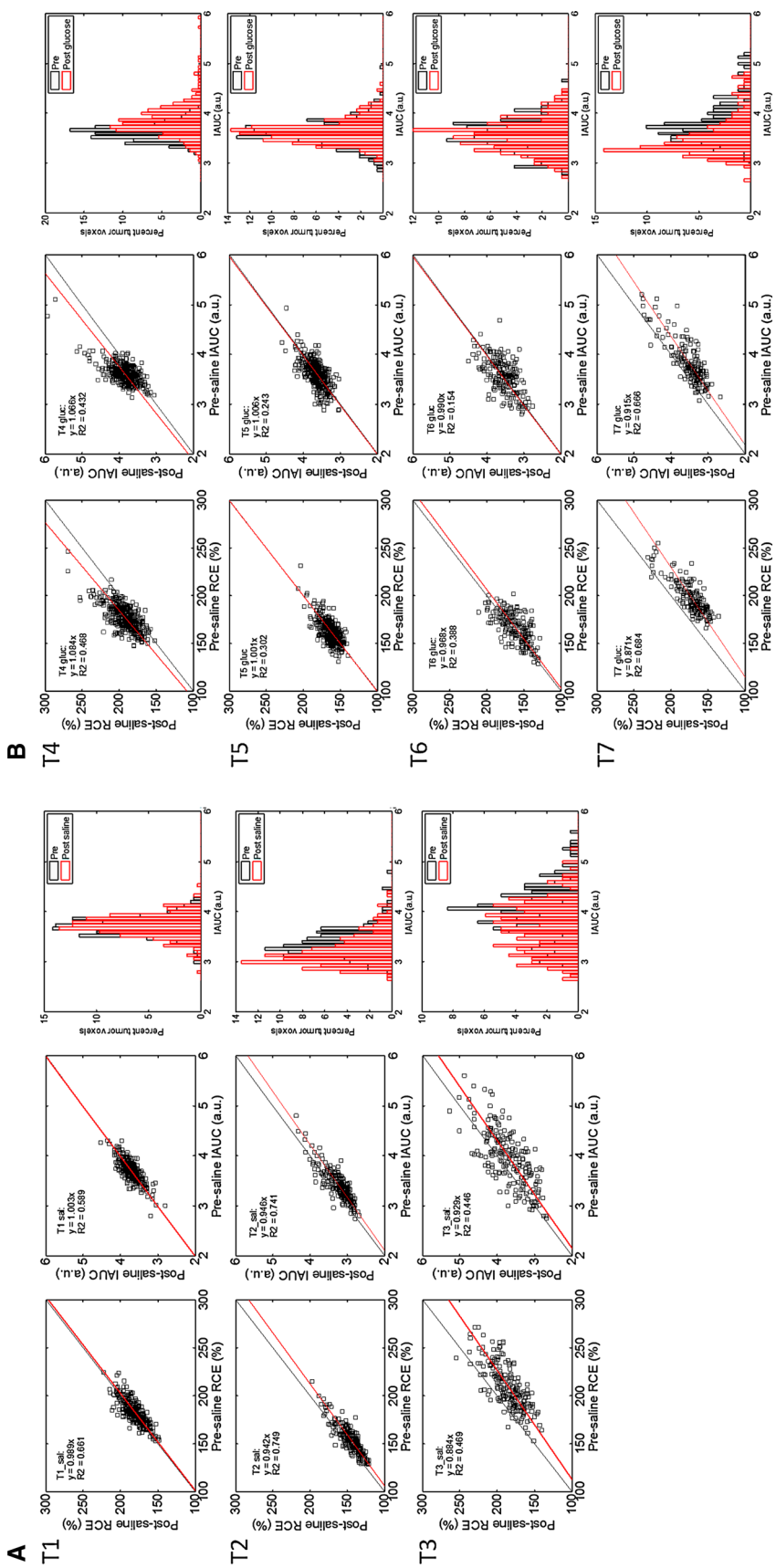

Fig. 3 Individual pixel-by-pixel correlation plots and histograms, for RCE and IAUC, pre-injection and post-injection of saline (**a**, tumors T1, T2 and T3) and glucose (**b**, tumors T4, T5, T6 and T7). Correlation plots (column 1, RCE; column 2, IAUC): identity lines (*black*) and linear regression lines (*red*) are shown for comparison, displaying the slope of linear regression (y) and Spearman's correlation coefficients (ρ) between pre-injection and post-injection data. Histograms for IAUC (column 3): *grey bars*, pre-injection; *red bars*, post-injection

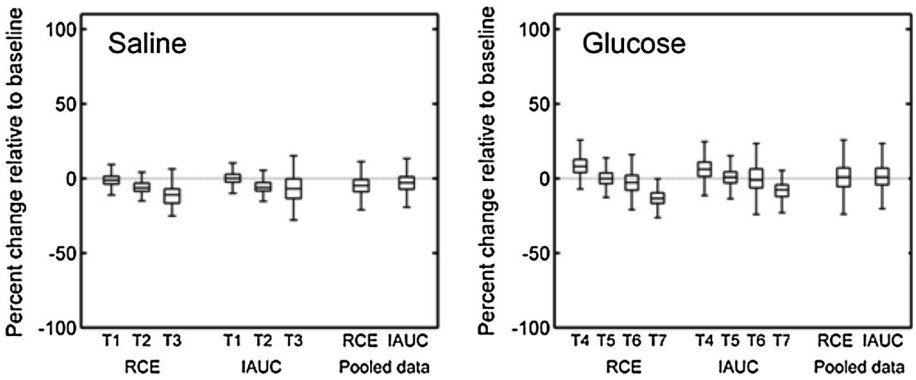

Fig. 4 *Box* plots of RCE and IAUC pixel changes during saline and glucose injections, for both individual tumors (1–7) and for pooled data within each group. *Lower* and *upper quartiles* represent the 25 and 75th percentiles, respectively, and whiskers indicate 0.35 % (*bottom*) and 99.65 % (*top*) of the distribution

perfusion/permeability that seemed to be more closely associated with the enhancement pattern of an individual tumor rather than the challenge. Averaged within each group, these RCE and IAUC parameters also showed small changes. It is difficult to ascertain whether RCE and IAUC are mostly measuring permeability or perfusion, or a combination of the two depending on the individual pixel investigated. Still, these surrogate parameters for permeability/perfusion do not significantly change with hyperglycemia under slight hypothermia in the investigated system.

Our results indicate that the protocol described in Ref. [6] for inducing hyperglycemia in GL261-bearing mice during moderate brain hypothermia by intraperitoneal injection of glucose does not lead to large changes in the vascular supply and permeability of these tumors. This is not surprising for several reasons. A relatively low dose of intraperitoneally injected glucose was used in those experiments (2.7 g/kg) [5, 6] compared to previous studies on rats (6–7.2 g/kg) [8–10]. Although a similar dose (2.5 g/kg) caused a 42 % decrease in blood flow of mouse fibrosarcomas [7], other studies of C6 rat gliomas showed that the post-glucose TBF decreases are considerably smaller in intracerebral tumors (20 %) than in subcutaneous tumors (80 %) [21]. Moreover, while halothane anesthesia, which was used in most previously published reports [8–10], decreases TBF; isoflurane (used in Refs. [5, 6]) has been shown to have no effect on this parameter [22]. Finally, no changes in intratumoral temperature were detected after administration of glucose [6], which suggests that the potential changes in tumor energy metabolism were small.

Moderate brain hypothermia ($\sim$30 °C) itself has been shown to decrease cerebral blood flow in different animals with selective regional patterns [23], perhaps through similar effects as those proposed for hyperglycemia [24]. Since the animals were exposed to moderate brain hypothermia for more than 4 h, the perfusion/permeability may have decreased mainly due to hypothermia, even before the glucose challenge. The effects of moderate hypothermia in the physiology of the GL261 tumors therefore remain unclear and should merit further attention.

Conclusion

Acute hyperglycemia induced by an intraperitoneal injection of glucose caused only small changes in vascular delivery to GL261 tumors kept at moderate hypothermia. In mice injected with either glucose or saline, the changes in the mean tumor values of RCE and IAUC parameters were small and did not exceed 13 %. These changes were non-significant within either the glucose or saline injection group, and may have been due to prolonged hypothermia rather than glycemic challenge.

Acknowledgments The authors would like to thank Ms. Milena Acosta for help in generating GL261 tumor-bearing mice. This work was funded by PHENOIMA—MICINN SAF 2008-0332, MARESCAN-SAF2011-23870; MICINN CDTI-CENIT (AMIT project); *Centro de Investigación Biomédica en Red–Bioingeniería, Biomateriales y Nanomedicina* (CIBER-BBN, [http://www.ciber-bbn.es/en]), an initiative of the Instituto de Salud Carlos III (Spain) co-funded by EU FEDER funds; IMAFEN (2008–2009), PROGLIO (2010–2011), PROGLIO2 (2012–2013) and MOLGLIO (2014–2015) intramural projects of CIBER-BBN.

References

1. Borges AR, Lopez-Larrubia P, Marques JB, Cerdan SG (2012) MR imaging features of high-grade gliomas in murine models: how they compare with human disease, reflect tumor biology, and play a role in preclinical trials. AJNR Am J Neuroradiol 33(1):24–36
2. Provent P, Benito M, Hiba B, Farion R, Lopez-Larrubia P, Ballesteros P, Rémy C, Segebarth C, Cerdán S, Coles JA, García-Martín ML (2007) Serial in vivo spectroscopic nuclear magnetic resonance imaging of lactate and extracellular pH in rat gliomas shows redistribution of protons away from sites of glycolysis. Cancer Res 67(16):7638–7645
3. Hamans B, Navis AC, Wright A, Wesseling P, Heerschap A, Leenders W (2013) Multivoxel 1H MR spectroscopy is superior

to contrast-enhanced MRI for response assessment after anti-angiogenic treatment of orthotopic human glioma xenografts and provides handles for metabolic targeting. Neuro Oncol 15(12):1615–1624
4. Simões RV, Ortega-Martorell S, Delgado-Goñi T, Fur YL, Pumarola M, Candiota AP, Martín J, Stoyanova R, Cozzone PJ, Juliá-Sapè M, Arús C (2012) Improving the classification of brain tumors in mice with perturbation enhanced (PE)-MRSI. Integr Biol (Camb) 4(2):183–191
5. Simões RV, García-Martín ML, Cerdán S, Arús C (2008) Perturbation of mouse glioma MRS pattern by induced acute hyperglycemia. NMR Biomed 21(3):251–264
6. Simões RV, Delgado-Goñi T, Lope-Piedrafita S, Arús C (2010) 1H-MRSI pattern perturbation in a mouse glioma: the effects of acute hyperglycemia and moderate hypothermia. NMR Biomed 23(1):23–33
7. Vaupel PW, Okunieff PG (1988) Role of hypovolemic hemoconcentration in dose-dependent flow decline observed in murine tumors after intraperitoneal administration of glucose or mannitol. Cancer Res 48(24 Pt 1):7102–7106
8. Hwang YC, Kim SG, Evelhoch JL, Seyedsadr M, Ackerman JJ (1991) Modulation of murine radiation-induced fibrosarcoma-1 tumor metabolism and blood flow in situ via glucose and mannitol administration monitored by 31P and 2H nuclear magnetic resonance spectroscopy. Cancer Res 51(12):3108–3118
9. Calderwood SK, Dickson JA (1980) Effect of hyperglycemia on blood flow, pH, and response to hyperthermia (42 degrees) of the Yoshida sarcoma in the rat. Cancer Res 40(12):4728–4733
10. Sevick EM, Jain RK (1988) Blood flow and venous pH of tissue-isolated Walker 256 carcinoma during hyperglycemia. Cancer Res 48(5):1201–1207
11. Jain RK, Shah SA, Finney PL (1984) Continuous noninvasive monitoring of pH and temperature in rat Walker 256 carcinoma during normoglycemia and hyperglycemia. J Natl Cancer Inst 73(2):429–436
12. Simões RV, García-Martín ML, Delgado-Goñi T, Candiota AP, Lope-Piedrafita S, Pumarola M, Arús C (2009) Hot-spots in mouse brain gliomas detected by MRSI pattern perturbation and DCE-MRI. Magn Reson Mater Phy (MAGMA) 22(Supp 1):196
13. Rodriguez E, Simões RV, Roig A, Molins E, Nedelko N, Slawska-Waniewska A, Aime S, Arús C, Cabanas ME, Sanfeliu C, Cerdán S, García-Martín ML (2007) An iron-based T1 contrast agent made of iron-phosphate complexes: in vitro and in vivo studies. Magn Reson Mater Phy (MAGMA) 20(1):27–37
14. Simões RV, Martinez-Aranda A, Martín B, Cerdán S, Sierra A, Arús C (2008) Preliminary characterization of an experimental breast cancer cells brain metastasis mouse model by MRI/MRS. Magn Reson Mater Phy (MAGMA) 21(4):237–249
15. Ortuno JE, Ledesma-Carbayo MJ, Simoes RV, Candiota AP, Arus C, Santos A (2013) DCE@urLAB: a dynamic contrast-enhanced MRI pharmacokinetic analysis tool for preclinical data. BMC Bioinformatics 14(1):316
16. Evelhoch JL (1999) Key factors in the acquisition of contrast kinetic data for oncology. J Magn Reson Imaging 10(3):254–259
17. Robinson SP, McIntyre DJ, Checkley D, Tessier JJ, Howe FA, Griffiths JR, Ashton SE, Ryan AJ, Blakey DC, Waterton JC (2003) Tumour dose response to the antivascular agent ZD6126 assessed by magnetic resonance imaging. Br J Cancer 88(10):1592–1597
18. Cha S, Johnson G, Wadghiri YZ, Jin O, Babb J, Zagzag D, Turnbull DH (2003) Dynamic, contrast-enhanced perfusion MRI in mouse gliomas: correlation with histopathology. Magn Reson Med 49(5):848–855
19. Collins DJ, Padhani AR (2004) Dynamic magnetic resonance imaging of tumor perfusion. Approaches and biomedical challenges. IEEE Eng Med Biol Mag 23(5):65–83
20. Johansen R, Jensen LR, Rydland J, Goa PE, Kvistad KA, Bathen TF, Axelson DE, Lundgren S, Gribbestad IS (2009) Predicting survival and early clinical response to primary chemotherapy for patients with locally advanced breast cancer using DCE-MRI. J Magn Reson Imaging 29(6):1300–1307
21. Ross BD, Mitchell SL, Merkle H, Garwood M (1989) In vivo 31P and 2H NMR [corrected] studies of rat brain tumor pH and blood flow during acute hyperglycemia: differential effects between subcutaneous and intracerebral locations. Magn Reson Med 12(2):219–234
22. Zhao M, Fortan LG, Evelhoch JL (1995) The effects of isoflurane and halothane on blood flow and 31P NMR spectra in murine RIF-1 tumors. Magn Reson Med 33(5):610–618
23. Strauch JT, Haldenwang PL, Mullem K, Schmalz M, Liakopoulos O, Christ H, Fischer JH, Wahlers T (2009) Temperature dependence of cerebral blood flow for isolated regions of the brain during selective cerebral perfusion in pigs. Ann Thorac Surg 88(5):1506–1513
24. Sevick EM, Jain RK (1991) Effect of red blood cell rigidity on tumor blood flow: increase in viscous resistance during hyperglycemia. Cancer Res 51(10):2727–2730